J. KSIAM **Vol.6**, No.2, 9-24, 2002

MULTIGRID METHOD FOR TOTAL VARIATION IMAGE DENOISING

MUN S. HAN AND JUN S. LEE

Abstract. Total Variation(TV) regularization method is effective for reconstructing "blocky", discontinuous images from contaminated image with noise. But TV is represented by highly nonlinear integro-differential equation that is hard to solve. There have been much effort to obtain stable and fast methods. C. Vogel introduced "the Fixed Point Lagged Diffusivity Iteration", which solves the nonlinear equation by linearizing. In this paper, we apply multigrid(MG) method for cell centered finite difference (CCFD) to solve system arise at each step of this fixed point iteration. In numerical simulation, we test various images varying noises and regularization parameter α and smoothness β which appear in TV method. Numerical tests show that the parameter β does not affect the solution if it is sufficiently small. We compute optimal α that minimizes the error with respect to L^2 norm and H^1 norm and compare reconstructed images.

1. Introduction

It is well known that recovering an image from a contaminated image is mathematically ill-posed. Rudin, Osher, and Fatemi [13] considered Total Variation(TV) regularization, which can effectively recover edges of an image and is one of the most successful regularization approaches. Computational experiments and mathematical analysis [8] have shown that this approach works well for recovering "blocky" image that is almost piecewise constant with jump discontinuities or sharp gradients separating regions where it is nearly constant. But TV regularization includes highly nonlinear part. Vogel and Oman introduced Lagged Diffusivity Fixed Point iteration method to linearize nonlinear problem which is very robust [17]. On the other hand, cell centered finite differences method is one of the most effective method for numerical solution of second order elliptic boundary value problems[9, 7, 18]. This has been used as the discretization for the image reconstruction problem. Multigrid methods can be used to solve the discrete systems arising from certain positive definite elliptic PDEs, like

2000 Mathematics Subject Classification: Primary 65N30, secondary 65F10
Keywords and phrases: multigrid methods, total variation regularization, cell-centered finite
This work supported by ETRI

Poisson's equation with $O(n)$ complexity (n is the number of pixels in the images or unknowns) [12] and its efficiency is shown in [1, 2]. For example, the complexity $O(n)$ of multigrid is contrast with complexity $O(n^{\frac{3}{2}})$ of direct band method. Multigrid method is influenced by choice of prolongation operator. We choose a weighted prolongation operator for multigrid algorithm applied to CCFD [7, 18]. In this paper, we shall consider TV regularization to present effective denoising formula, Lagged Diffusivity Fixed Point Iteration method to linearize nonlinear denoising problem which is expressed by TV regularization, and cell centered finite difference method for discretization and multigrid method to solve system on each iteration step.

The rest of this paper is organized as follows. In section 2, we introduce Total Variation Regularization(TVR) and 'Lagged Diffusivity Fixed Point iteration method'. In section 3, we introduce cell centered finite difference methods. In section 4, we introduce multigrid algorithm for it. In section 5, we test several images including 'Lena' with varying α and noises. Numerical tests show that the parameter β does not affect the solution if it is sufficiently small. We consider optimal α that minimizes the error with respect to L^2 norm and H^1 norm and compare reconstructed images.

2. Total variation regularization

The relation between noisy image and original image can be expressed mathematically by

$$z = u + n \tag{2.1}$$

where u represents the desired true solution, n represents the noise, and z represents the observed data. The noise is assumed to be a Gaussian white noise, *i.e.*, the values $u(x, y)$ are uncorrelated random variables with a normal distribution with mean 0 and variance σ^2 for all $(x, y) \in \Omega$ and a uniform noise, *i.e.*, the values $u(x, y)$ are uncorrelated random variables with a uniform distribution on the interval $(-2\sigma, 2\sigma)$. It is known that the image reconstruction is mathematically ill-posed. One needs other suitable constraint. Rudin, Osher, and Fatemi [13] considered the constrained minimization problem,

$$\min_u \int_\Omega |\nabla u|\, dx \quad \text{subject to} \quad \| u - z \|^2 = \sigma^2, \tag{2.2}$$

where the parameter σ describes the magnitude of the noise n in the data in the model equation (2.1). Here Ω is a bounded, convex region in d-dimensional space, $|\cdot|$ denotes the Euclidean norm in R^d, and $\|\cdot\|$ denotes the norm on $L^2(\Omega)$. Vogel *et al.* [17] consider a closely related problem - the unconstrained minimization of the TV-Penalized least squares functional instead of imposing the constraint explicitly, which is described as follows:

$$f(u) = \frac{1}{2} \| u - z \|^2 + \alpha J_\beta(u), \tag{2.3}$$

where

$$J_\beta(u) = \int_\Omega \sqrt{|\nabla u|^2 + \beta^2}\, dx \tag{2.4}$$

and α, β are (typically small) positive parameters. The parameter α controls the tradeoff between goodness of fit to the data, as measured by $\| u - z \|$, and the variability of the solution, measured by $J_\beta(u)$. When $\beta = 1$, $J_\beta(u)$ represents the surface area of the graph of u, while $\beta = 0$ gives the total variation of u. When $\beta = 0$, TV-penalized least squares can be viewed as a penalty method [11] to solve the constrained problem (2.2). The penalty parameter α in (2.3) is inversely proportional to the Lagrange multiplier for (2.2). This penalty approach is standard in the inverse problems community, and is commonly referred to as Tikhonov regularization. Provided the parameters are selected appropriately, the solutions obtained by these two methods are identical. However, from a computational standpoint, unconstrained problems are much easier to implement than constrained problems. To minimize $f(u)$ in (2.3), we will need its gradient. By using integration by parts with Neumann boundary condition on (2.3), it can be shown that the gradient of the TV functional is

$$\nabla TV(u) = -\nabla \cdot \left(\frac{\nabla u}{\sqrt{|\nabla u|^2 + \beta^2}} \right).$$

Thus, the first order optimality condition for the problem (2.3) is given by

$$\begin{aligned} \nabla f(u) = g(u) = -\alpha \nabla \cdot \left(\frac{\nabla u}{\sqrt{|\nabla u|^2 + \beta^2}}\right) + u - z = 0, \quad x \in \Omega, \\ \frac{\partial u}{\partial n} = 0, \quad x \in \partial\Omega. \end{aligned} \tag{2.5}$$

This is what we need to solve to find the restored image u. C. Vogel *et al.* [17] propose the Fixed Point Lagged Diffusivity Iteration to solve the optimality equation (2.5). This method consists in linearizing the nonlinear differential term in (2.5) by lagging the diffusion coefficient $(\frac{1}{\sqrt{|\nabla u|^2+\beta^2}})$ behind one iteration. Thus u^{k+1} is obtained as the solution to the linear integro differential equation

$$(u^{k+1} - \alpha \nabla \cdot (\frac{\nabla\, u^{k+1}}{\sqrt{|\nabla u^k|^2 + \beta^2}})) = z.$$

This can be interpreted within the framework of generalized Weiszfeld's methods, as introduced in [15]. As proved in that paper, this method is monotonically convergent, in the sense that the objective function evaluated at the iterates forms a monotonically decreasing sequence, and that the convergence rate as linear. While the rate of convergence is only linear, the iteration seems to be globally convergent (i.e., it always converges, no matter what the initial guess). Moreover, the convergence is far more rapid than that of gradient descent (see [17]). In practice, this method is very robust. Thus we will apply this method for our purpose.

3. Cell-centered finite difference discretization for TVR

Here, we briefly introduce CCFD. We assume that $\rho(\nabla u) = \dfrac{1}{\sqrt{|\nabla u|^2 + \beta^2}}$ are known. Consider the linearized model problem :

$$\begin{aligned} u^{l+1} - \nabla \cdot \left(\rho(\nabla u^l) \nabla u^{l+1} \right) &= z \text{ in } \Omega, \\ \frac{\partial u^{l+1}}{\partial n} &= 0 \text{ on } \partial\Omega, \end{aligned} \tag{3.1}$$

where Ω is the unit square. Let N_x and N_y denote the number of equispaced partitions in the x and y directions where $N_x = N_y = 2^k$ for $k = 1, 2, \ldots, m$ and $h_x = \frac{1}{N_x}$, $h_y = \frac{1}{N_y}$. For simplicity, let $N = N_x = N_y$, $h = h_x = h_y$. Then the total number of cells(subsquare in Ω) is given by $N \times N$. Let $\{\Omega^k\}$ and $\Omega^k_{ij},\ i, j = 0, \ldots, N-1$ denote subdivisions and cell for level k. The cell centers are given by (x_i, y_i) where

$$\begin{aligned} x_i &= (i - \frac{1}{2})h, \\ y_j &= (j - \frac{1}{2})h. \end{aligned}$$

The midpoints of the cell edges are given by $(x_{i\pm\frac{1}{2}}, y_j)$ and $(x_i, y_{j\pm\frac{1}{2}})$, where

$$\begin{aligned} x_{i\pm\frac{1}{2}} &= x_i \pm \frac{h}{2}, \\ y_{j\pm\frac{1}{2}} &= y_j \pm \frac{h}{2}. \end{aligned} \tag{3.2}$$

Let V_k denote the space of functions that are piecewise constant on each cell for $k = 1, 2, \ldots, m$. CCFD is obtained by first integrating (3.1) formally against test functions ϕ_{ij} on V_k, where $\phi_{ij} = 1$ on Ω^k_{ij} and $\phi_{ij} = 0$ elsewhere. Integrating by parts, we obtain

$$\int_{\Omega^k_{ij}} u^{l+1} d\Omega - \int_{\partial\Omega^k_{ij}} \rho(\nabla u^l) \frac{\partial u^{l+1}}{\partial n}\, ds = \int_{\Omega^k_{ij}} z\, dx \tag{3.3}$$

for $i, j = 1, \ldots, n$. Now we will approximate the normal derivative $\dfrac{\partial u^{l+1}}{\partial n}$ on the edges by the difference quotient of a function $u \in V_k$. Then we have

$$\rho(\nabla u^l)_{i,j+\frac{1}{2}} \frac{u^{l+1}_{i,j+1} - u^{l+1}_{i,j}}{h},$$

where $h = h_k = 1/2^k$, and $u^{l+1}_{i,j} = u^{l+1}(x_i, y_j)$ (and similarly for other subscripted u). Similarly, we obtain others normal derivatives $\frac{\partial u^{l+1}}{\partial n}$ and the diffusion coefficients

$$
\begin{array}{ccccc}
(i_1, j^1) & & (i, j^1) & & (i^1, j^1) \\
& (I_2, J^1) & (I_1, J^1) & (I, J^1) & (I^1, J^1) \\
& (I_2, J) & (I_1, J) & (I, J) & (I^1, J) \\
(i_1, j) & & (i, j) & & (i^1, j) \\
& (I_2, J_1) & (I_1, J_1) & (I, J_1) & (I^1, J_1) \\
& (I_2, J_2) & (I_1, J_2) & (I, J_2) & (I^1, J_2) \\
(i_1, j_1) & & (i, j_1) & & (i^1, j_1)
\end{array}
$$

FIGURE 1. *Elements $E^k_{i,j}$s and their subdivision* ; $I_1 = I - 1, J^1 = J + 1$, etc.

$\rho(\nabla u^l)_{i+\frac{1}{2},j}$ on the common edges. Next, we approximate the third term in (3.3) as follows by using mid-point quadrature rule:

$$\int_{\Omega^k_{ij}} u^{l+1} d\Omega = u^{l+1}_{i,j} h^2. \tag{3.4}$$

We have finite difference equations as follows:

$$
\begin{aligned}
&\left[\rho(\nabla u^l)_{i-\frac{1}{2},j} + \rho(\nabla u^l)_{i+\frac{1}{2},j} + \rho(\nabla u^l)_{i,j-\frac{1}{2}} + \rho(\nabla u^l)_{i,j+\frac{1}{2}} + 4h^2\right] u^{l+1}_{i,j} \\
&\quad -\rho(\nabla u^l)_{i-\frac{1}{2},j} u^{l+1}_{i-1,j} - \rho(\nabla u^l)_{i+\frac{1}{2},j} u^{l+1}_{i+1,j} \\
&\quad -\rho(\nabla u^l)_{i,j-\frac{1}{2}} u^{l+1}_{i,j-1} - \rho(\nabla u^l)_{i,j+\frac{1}{2}} u^{l+1}_{i,j+1} = h^2 z_{i,j}.
\end{aligned} \tag{3.5}
$$

When one of the edges coincides with the boundary of Ω, consider Neumann boundary condition, i.e. $\frac{\partial u}{\partial n} = 0$ on $\partial\Omega$. After dividing the resulting equation by h^2, we obtain a system of linear equation of the form

$$A_k(\nabla u^l)\, u^{l+1} = z \tag{3.6}$$

where $A_k(\nabla u^l)$ is a typical sparse, $N^2 \times N^2$ symmetric, positive definite matrix similar to those arising in the vertex finite difference method.

4. Multigrid algorithm for cell-centered method

Our scheme is the fixed point lagged diffusivity iteration i.e., we solve the nonlinear model equation by linearizing and updating u^{l+1} from solving the linear equation $A(\nabla u^l)u^{l+1} = z$. So, here in this section, we consider the linear multigrid for the cell-centered finite difference method and state some results on the mutigrid algorithm. Let $\{V_k\}$ be the sequence of function space, for $k = 1, 2, \ldots, J$. We define two quadratic forms $A_k(\cdot,\cdot)$ and $(\cdot,\cdot)_k$ on $V_k \times V_k$ by

$$(u, v)_k = h_k^2 \sum_{i,j}^{n} u_{i,j} v_{i,j}$$

and

$$A_k(u, v) = (A_k u, v) = h_k^2 \sum_{i,j}^{n} (A_k u)_{i,j} v_{i,j}.$$

We assume a certain prolongation operator $I_{k-1}^k : V_{k-1} \to V_k$ for $k = 2, \ldots, J$ and define the restriction operator $I_k^{k-1} : V_k \to V_{k-1}$ as its adjoint with respect to $(\cdot,\cdot)$:

$$(I_k^{k-1} u, v) = (u, I_{k-1}^k), \quad \forall u \in V_k, v \in V_{k-1}.$$

Multigrid algorithm gives rise to iterative procedures for the solution $u \in V_k$ satisfying (3.6). Let $\{R_k\}$ be a sequence of linear smoothing operators $R_k : V_k \to V_k$ for $k = 2, \ldots, J$ and set

$$R_k^{(l)} = \begin{cases} R_k, & \text{if } l \text{ is odd,} \\ R_k^T, & \text{if } l \text{ is even.} \end{cases}$$

Let $K_k = I - R_k A_k$ on V_k. Then we note $K_k^* = I - R_k^T A_k$. Here, 'T' and '$*$' denote adjoint with respect to $(\cdot,\cdot)_k$ and $A_k(\cdot,\cdot)$, respectively. Let $B_k : V_k \to V_k$ be multigrid operator. Now we will define multigrid algorithm as follows :

Multigrid Algorithm V(m,m)

Set $B_1 = A_1^{-1}$. Assume that B_{k-1} has been defined and define $B_k z$ for $z \in V_k$ as follows :

Step 1.**:** Set $v^0 = 0$ and $q^0 = 0$.

Step 2. **(Pre - relaxation):** Define v^i for $i = 1, 2, \ldots, m$ by

$$v^i = v^{i-1} + R_k^i (z - A_k v^{i-1}).$$

Step 3.**:** Define $w^m = v^m + I_{k-1}^k q$ and q is defined by

$$q = B_{k-1}[I_k^{k-1}(z - A_k v^m)].$$

Step 4. **(Post - relaxation):** Define w^i for $i = m+1, \ldots, 2m$ by

$$w^i = w^{i-1} + R_k^{(i+m)} (z - A_k w^{i-1}).$$

Step 5.**:** Set $B_k z = w^{2m}$.

Here, m is the number of smoothings which may vary depending on k but we consider the fixed $m = 1$. For the smoother, we will adopt Gauss-Seidel method. For the prolongation operator, we will use the bilinear prolongation. Recently, Kwak[7] devised a new prolongation and showed V-cycle multigrid convergence. The bilinear prolongation has similar properties as that in [7]. Let $\Omega_{i,j}^{k-1}$ be a cell at level $k-1$ and $u_{i,j}^{k-1}$ be the value at the center of $\Omega_{i,j}^{k-1}$. Let $u_{I,J}^{k+1}$ be the value at the upper right subcell of $\Omega_{i,j}^{k-1}$, $u_{I,J+1}^{k+1}$ be the value at the upper left subcell of $\Omega_{i,j+1}^{k-1}$, $u_{I+1,J}^{k+1}$ be the value at the lower right subcell of $\Omega_{i+1,j}^{k-1}$, and $u_{I+1,J+1}^{k+1}$ be the value at the lower left subcell of $\Omega_{i+1,j+1}^{k-1}$. Define $I_{k-1}^{k} : V_{k-1} \to V_k$ by $u^k = I_{k-1}^{k} u^{k-1}$ as follows :

$$
\begin{aligned}
u_{I,J}^{k} &= \frac{9u_{i,j}^{k-1} + 3u_{i,j+1} + 3u_{i+1,j} + u_{i+1,j+1}}{16},\\
u_{I,J+1}^{k} &= \frac{3u_{i,j}^{k-1} + 9u_{i,j+1} + 3u_{i+1,j} + u_{i+1,j+1}}{16},\\
u_{I+1,J}^{k} &= \frac{3u_{i,j}^{k-1} + u_{i,j+1} + 9u_{i+1,j} + 3u_{i+1,j+1}}{16},\\
u_{I+1,J+1}^{k} &= \frac{u_{i,j}^{k-1} + 3u_{i,j+1} + 3u_{i+1,j} + 9u_{i+1,j+1}}{16}.
\end{aligned}
$$

Now we consider the generation of $A_k(\nabla u^l)$ for $k = 1, \ldots, J$. At the top level, i.e., $k = J$, we will generate $\rho(\nabla u^l)_{i,j+\frac{1}{2}}$, $\rho(\nabla u^l)_{i,j-\frac{1}{2}}$, $\rho(\nabla u^l)_{i+\frac{1}{2},j}$ and $\rho(\nabla u^l)_{i-\frac{1}{2},j+\frac{1}{2}}$ from neighboring points of $u_{i,j}^l$ at the level J as in the previous discussion. At the next level $k = J-1$, we first generate $u_{i,j}^l$ at level $k = J-1$ from $u_{i,j}^l$ at level $k = J$ by using the projection operator I_k^{k-1} which is defined as the transpose of the prolongation operator I_{k-1}^{k}. In this way, we will construct $A_k(\nabla u^l)$ for $k = 1, \ldots, J$.

5. Numerical result

In implementation, one have to compute the diffusion coefficient $\rho(\nabla u) = \alpha/\sqrt{\beta^2 + |\nabla u|^2}$ from the known date u.

$$
|\nabla u_{i-\frac{1}{2},j}|^2 = (\frac{\partial}{\partial x} u_{i-\frac{1}{2},j})^2 + (\frac{\partial}{\partial y} u_{i-\frac{1}{2},j})^2.
$$

First, we approximate each partial derivatives as follows:

$$
\begin{aligned}
\frac{\partial}{\partial x} u_{i-\frac{1}{2},j} &\approx \frac{u_{i-1,j} - u_{i,j}}{h},\\
\frac{\partial}{\partial y} u_{i-\frac{1}{2},j} &\approx \frac{1}{2}(\frac{u_{i,j+1} - u_{i,j-1}}{2h} + \frac{u_{i-1,j+1} - u_{i-1,j-1}}{2h}).
\end{aligned}
$$

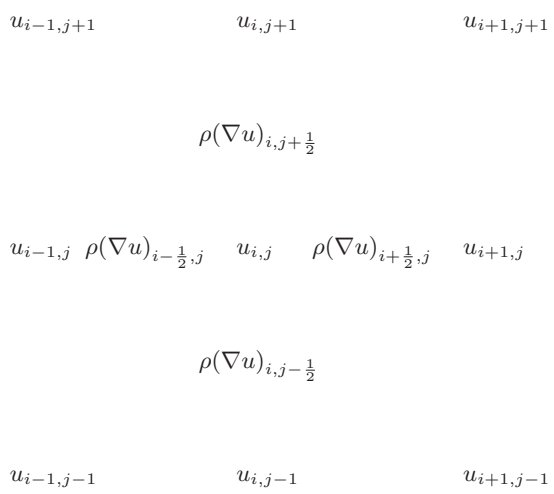

FIGURE 2. cell-centers $u_{i,j}$ and the diffusion $\rho(\nabla u)_{i,j+\frac{1}{2}}$, etc.

Then we can get $\rho(\nabla u)_{i-\frac{1}{2},j}$. Similarly, we have $\rho(\nabla u)_{i+\frac{1}{2},j}$, $\rho(\nabla u)_{i,j-\frac{1}{2}}$, $\rho(\nabla u)_{i,j+\frac{1}{2}}$ on the common edges.

All the images in this experiment have 256×256 pixels and are black and white images. We performed an experiment with original pictures (Figure 4-(a) and 6-(a)) and contaminated image with noise (Figure 4-(b), 5-(b), 6-(b) and 7-(b)). We consider pictures with Gaussian noise of $\sigma = 10$ and $\sigma = 20$.

For the parameter β, numerical results show that β does changes little only if it is small enough(β is less than 10^-3). For example in Figure 3, we present the recovered images fixed $\alpha = 8\times10^{-3}$ varying $\beta = 10^{-3}, 10^{-5}, 10^{-7}, 10^{-9}$ and they are almost same. Since β is not sensitive, we performed experiment with fixed $\beta = 10^{-6}$.

So, hereafter, we consider the optimality of α. We present recovered images with α which minimizes the L^2 and H^1 error between the original image and the recovered image. In Figure $4 \sim 7$, we compare images with all αs which are recovered by using the L^2-norm with those obtained by the gradient norm. Here, we assume that we know the original images and noise is Gaussian noise.

	Figure number	Gaussian noise of $\sigma = 10$	Gaussian noise of $\sigma = 20$
L^2 norm	Figure 4-(c) and 5-(c)	6.5×10^{-3}	3.0×10^{-2}
	Figure 6-(c) and 7-(c)	2.0×10^{-3}	1.5×10^{-2}
H^1 norm	Figure 4-(d) and 5-(d)	1.55×10^{-2}	5.5×10^{-2}
	Figure 6-(d) and 7-(d)	1.8×10^{-2}	5.0×10^{-2}

TABLE 1. the optimal values of α according to the amount of noise

Figure 4-(a) is original Lena and Figure 4-(b) is noisy image (with Gaussian noise of $\sigma = 10$). Figure 4-(c) and Figure 4-(d) are denoised images with optimal αs in L^2 norm and gradient norm sense.
Figure 5-(a) is original Lena and Figure 5-(b) is noisy image (with Gaussian noise of $\sigma = 20$). Figure 5-(c) and Figure 5-(d) are denoised images with optimal αs in L^2 norm and gradient norm sense.

Figure 4-(d) and 5-(d) are more clear than Figure 4-(c) and 5-(c). Figure 6-(a) is original Lab member's picture and Figure 6-(b) is noisy image (with Gaussian noise of $\sigma = 10$). Figure 6-(c) and Figure 6-(d) are denoised image with optimal α in L^2 norm and gradient norm sense.
Figure 7-(a) is original Lab member's picture and Figure 7-(b) is noisy image (with Gaussian noise of $\sigma = 20$). Figure 7-(c) and Figure 7-(d) are denoised image with optimal α in L^2 norm and gradient norm sense.

All optimal values of αs at each picture are different. But they follow a pattern. The optimal value of α is directly proportional to the amount of noise (See Table 1). In the process of denoising an incident occur. A sharp and delicate edges tend to blunt. Our denoising experiment is more effective board part (for example, Lena's shoulder and background, and Word image (See Figure 4, 5, 6, 7) than delicate part (for example, hair of Lena in Figure $4 \sim 7$.

FIGURE 3. (a) Upper left is original Lena Image. (b) Upper right is noisy image with Gaussian noise of $\sigma = 20$. (c) $\alpha = 8 \times 10^{-3}$, $\beta = 1 \times 10^{-3}$ (d) $\alpha = 8 \times 10^{-3}$, $\beta = 1 \times 10^{-5}$ (e) $\alpha = 8 \times 10^{-3}$, $\beta = 1 \times 10^{-7}$ (f) $\alpha = 8 \times 10^{-3}$, $\beta = 1 \times 10^{-9}$.

FIGURE 4. (a)Upper left is original Lena Image. (b)Upper right is noisy image with Gaussian noise of $\sigma = 10$. (c)Lower left is denoising image with optimal values $\alpha = 6.5 \times 10^{-3}$, $\beta = 10^{-6}$ in L^2 norm sense. (d)Lower right is denoising image with optimal values$\alpha = 15.5 \times 10^{-3}$, $\beta = 10^{-6}$ in H^1 norm sense.

FIGURE 5. (a) Upper left is original Lena Image. (b) upper right is noisy image with Gaussian noise of $\sigma = 20$. (c) Lower left is denoising image with optimal values $\alpha = 3\times10^{-2},\ \beta = 10^{-6}$ in L^2 norm sense. (d) Lower right is denoising image with optimal values $\alpha = 5.5 \times 10^{-2},\ \beta = 10^{-6}$ in H^1 norm sense.

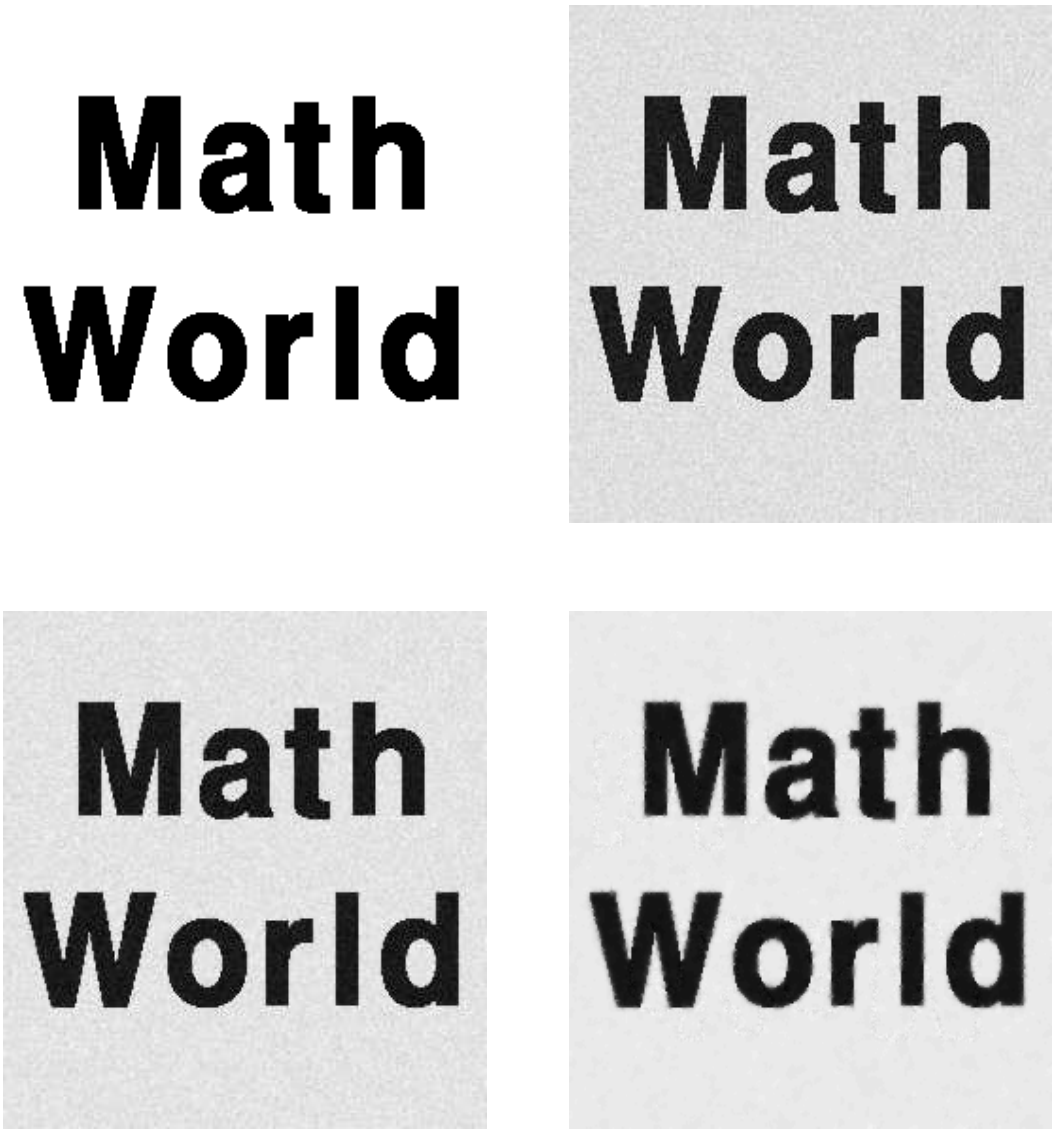

FIGURE 6. (a)Upper left is original word Image. (b)Upper right is noisy image with Gaussian noise of $\sigma = 10$. (c)Lower left is denoising image with optimal values $\alpha = 2.\times 10^{-3},\ \beta = 10^{-6}$ in L^2 norm sense. (d)Lower right is denoising image with optimal values$\alpha = 1.8 \times 10^{-2},\ \beta = 10^{-6}$ in H^1 norm sense.

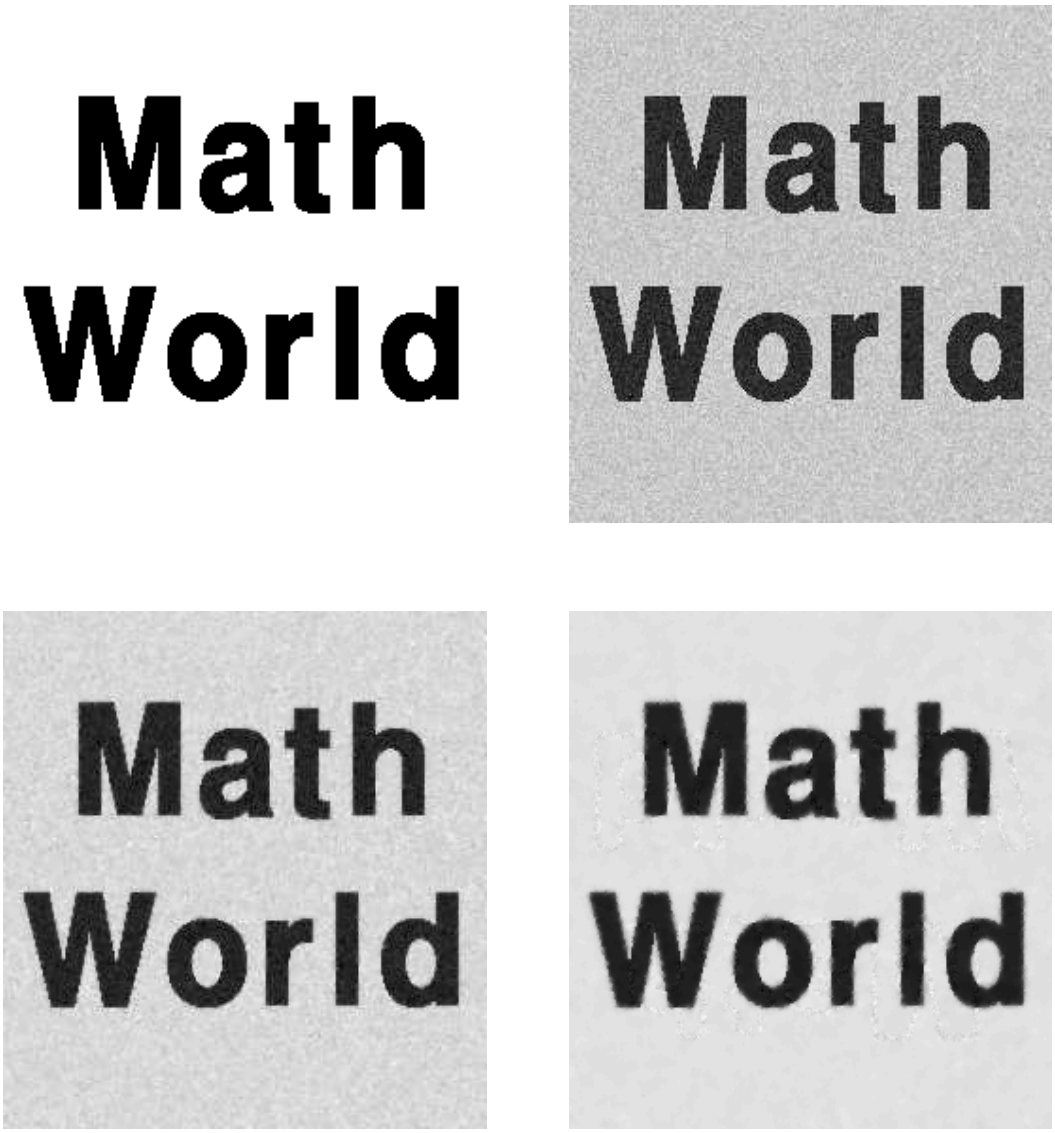

FIGURE 7. (a) Upper left is original word Image. (b) upper right is noisy image with Gaussian noise of $\sigma = 20$. (c) Lower left is denoising image with optimal values $\alpha = 1.5 \times 10^{-2}$, $\beta = 10^{-6}$ in L^2 norm sense. (d) Lower right is denoising image with optimal values $\alpha = 5. \times 10^{-2}$, $\beta = 10^{-6}$ in H^1 norm sense.

References

[1] J. H. Bramble and J. E. Pasciak, *New convergence estimates for multigrid algorithms*, Math. Comp., **49**(1987), 311–329.

[2] J. H. Bramble, J. E. Pasciak, and J. Xu, *The analysis of multigrid algorithms with onnested spaces or non inherited quadratic forms*, Math. Comp., **56**(1991), 1–34.

[3] R. H. Chan, T. F. Chan, and C. K. Wong, *Continuation method for total variation denoising problems*, in Advanced Signal processing algorithms, F. T. Luk, ed., vol. **2563**, SPIE - The Int'l Society for Optical Eng., 1995, 314–325.

[4] T. Chan, G. Golub, and P. Mulet, *A nonlinear primal dual method for Total Variation based image restoration*, in ICAOS'96, 12th Int'l Conf. on Analysis and Optimization of systems : Images, wavelets and PDE's, Paris, June 26-28, 1996, M. Berger, R. Deriche, I. Herlin, J.Jaffre, and J. Morel, eds., no. 219 in Lecture Notes in Control and Information Science, 1996, 241–252.

[5] T. F. Chan and P. Mulet, *Iterative Methods for Total Variation Image Restoration*, Proceedings of Winter School on Iterative Methods, the Chinese University of Hong Kong, Dec 1995, Spring Verlag, Singapore.

[6] T. Chan and C. Wong, *Total Variation Blind Deconvolution*, virtual Proc. of ONR workshop, Sep. 4-6 1996.

[7] Do Y. Kwak, *V-cycle multigrid for cell-centered finite differences*, SIAM J. Sci. Comput., 21(1999), 552–564.

[8] D. Dobson and F. Santosa, *Recovery of blocky images from noise and blurred data*, Tech. Report No. 94-7, Center for the Mathmatics of Waves, University of Delaware, 1994.

[9] R. E. Ewing and J. Shen, *A multigrid algorithm for the cell-centered finite difference schme*, in the Proceedingof the 6th Copper Mountain Conference on Multigrid Methods, April 1993, NASA Conference Publication 3224.

[10] Y. Li and F. Santosa, *An affine scaling algorithm for minimizing total variation in image enhancement*, tech. report CTC94TR201, Cornell Theory Center, Cornell University.

[11] D. Luenberger, *Introduction to Linear and Nonlinear Programming*, Addison-Wesley, 1965.

[12] S. F. McComick, *Multigrid Method*, Society for Industrial and Applied Mathmetics Philadelphia Pennsylvania (1987).

[13] L. I. Rudin, S. Osher, and E. Fatemi, *Nonlinear Total Variation Based Noise Removal Algorithms*, Physica D, vol **60**(1992), 259–268.

[14] C. R. Vogel, *A multigrid method for total variation-based image denoising*, in Computation and Control IV, K.Bowers and J. Lund, eds., vol. **20** of Progress in Systems and Control Theory, Birkhauser, 1995.

[15] H. Voss and U. Eckhardt, *Linear convergence of generalized Weiszfeld's method*, Computing, **25** (1980).

[16] C. R. Vogel and M. E. Oman, *Fast numerical methods for total variation minimization in image reconstruction*, proceedings of SPIE 1995, San Diego, Advanced Signal Processing Algorithms, vol. **2563**, edited by F. T. Luk.

[17] C. R. Vogel and M. E. Oman, *Iterative Methods for Total Variation Denoising*, SIAM J. Sci. Comput., **17** (1996), 227–238.

[18] P. Wesseling, *Cell centered multigrid for interface problems*, J. Comput. Phys., **79** (1988), 85–91.

ETRI,
Taejon, 305-350, KOREA
E-mail: msh@etri.re.kr
This work supported by ETRI.

Department of Mathematics
KAIST
Taejon, 305-701, KOREA
E-mail: jslee@math.kaist.ac.kr